Hidden Periodic Motions for Brushless Motor with Unsteady Torque Excitation

Jianzhe Huang and Fuhong Min

Abstract Due to the coupling between the direct-axis current, quadrature-axis current and rotor speed, the dynamic response could be strongly nonlinear. Besides, if the working condition is severe, the loading is no longer constant and multiple harmonics could be introduced. In this chapter, a 3-D model for brushless motor is discussed, and an excitation with single harmonic will be considered. With discrete implicit maps algorithm, complex dynamical behaviors can be obtained for such a brushless motor. With bifurcation analysis, the parameter sensitivity can be obtained which can be a suggestion for design and operation. This chapter is dedicated to Valentin Afraimovich for his fabulous achievement in the scientific world.

1 Introduction

A brushless motor is an important power source which can be used in various fields such as robotics and aerospace. The vibration of such a motor could affect the performance of the loading, the comfort of the environment, the fatigue life of the entire system etc. Therefore, vibration issues should be considered in the design stage of a brushless motor. Due to the variation of the rotor speed, it could cause the torsional vibration of the rotor system and then affect the vibration of the whole structure. Hemati [1, 2] formulated a mathematical model for a brushless motor in a rotating coordinate frame through Park's transformation to investigate the global and local dynamics of such a direct-drive brushless motor. Such a model of brushless motor is a set of three dimensional first order autonomous differential equations system. Kang et al. [3] applied nonideal trapezoidal back EMF to attenuate the undesired torque fluctuation for the brushless dc motor, and a high precision encoder was used to measure the instantaneous torque ripple. Rubaai et al. [4] constructed a three-layer feedforward network to identify and control brushless dc motor drives. The

J. Huang (✉) · F. Min
School of Aeronautics and Astronautics, Shanghai Jiao Tong University, Shanghai 200240, China

D. Volchenkov (ed.), *The Many Facets of Complexity Science*, Nonlinear Physical Science,
https://doi.org/10.1007/978-981-16-2853-5_6

differential equations for the stator current were transformed to a single second-order nonlinear differential equation, and the solution was worked out by second-order central difference approximation. In 2003, Ge and Chang [5] transformed the brushless motor system into a compact form to study the chaos synchronization of identical systems through four methods such as the adaptive control, the backstepping design method, the Gerschgorin theorem and the addition of a monitor. Lee and Ehsani [6] effectively analyzed the speed, torque, voltages and currents of PWM inverter components using a developed model based on MATLAB environment. The trapezoidal back EMF waveforms were modeled as a function of rotor position. Jabbar et al. [7] introduced a methodology of modeling and numerical simulation of BLDCM with time-stepping approach. Finite element method (FEM) was considered to be practical to compute the performance of electrical machines. The simulation results correlated well with the experimental results which indicated that the model was significant. Luo [8, 10] studied the application of the combination of dynamic surface control (DSC) technology, radial basis function (RBF) neural network, and adaptive method, in the control of chaos for the BLDCM system. The same model with Hemati was applied, and the tangent barrier Lyapunov function (TBLF) was used for a time-delay nonlinear system. Zhang et al. [9] investigated the boundedness solutions of BLDCM. The generalized Lyapunov function stability theory and the extremum principle of function were used to analyze global attractive and positively invariant sets. The efficiency has been verified through the numerical simulations. Jagiea and Gwozdz [11] introduced a time-periodic finite element model of a brushless dc motor to evaluate the machine characteristic and the power losses. Cho et al. [12] analyzed the vibration characteristics of a brushless direct current motor through an entire finite element model, and electromagnetic-structural weak coupled analysis was carried out to give the transient response.

In this chapter, a brushless motor will be expressed with a set of three-dimensional nonlinear different equations. The electrical states (quadrature-axis current and direct-axis current) and mechanical state (rotor speed) are coupled. In the history of development of techniques for solving the steady-state response analytically of a nonlinear system, perturbation method [13] and harmonic balance method [14] are two of the most famous methods, but small parameter assumption for nonlinear terms was made. In order to remove such a limitation and deal with systems with strong nonlinearity, a generalized harmonic balanced method was developed and the effectiveness of such a method was verified with the Duffy oscillator [15], nonlinear Jeffcott oscillator [16] etc. Further, a semi-analytic methodology called discrete implicit maps was introduced [17] to give the analytic solution of periodic motions for any type of nonlinear system which possesses ordinary differential equations. With such a method, the bifurcation of analytic steady state solution for nonlinear systems such as piston in a high pressure gas cylinder [18], hardening Duffing oscillator with time-delay [19] and Parametrically Excited Pendulum [20] etc. have been obtained.

Since such a discrete implicit map method can be easily applied to solve nonlinear systems, and the stability and bifurcation condition can also be accurately calculated with which a large dimension of sparse Jacobian matrix is avoided, the analytic solution of periodic motions for nonlinear equations for brushless motor system will

be calculated using such a technique herein. Additionally, the number of harmonic terms does not need to be determined before the calculation, thus the accuracy of the analytic solution can be guaranteed. For a brushless motor with loading, the loading can cause the torque fluctuation when the loading increases which may dramatically change the dynamic characteristics for brushless motor dramatically, for instance the steady state motion may become other type of periodic motion or chaos when the periodical torque is introduced.

2 Motion Discretization and Mapping Reconstruction for Periodic Motions

In Fig. 1, a three-phase brushless motor with drive circuit is illustrated. The relationship between the input voltage and the back EMF in the motor will be expressed as

$$\begin{aligned} u_a &= Ri_a + L\frac{di_a}{dt} + e_a, \\ u_b &= Ri_b + L\frac{di_b}{dt} + e_b, \\ u_c &= Ri_c + L\frac{di_c}{dt} + e_c. \end{aligned} \tag{1}$$

Through Park transformation and a periodical torque excitation is considered, the dynamical equations for such a brushless motor in the d-q coordinates can be expressed as

$$\frac{di_q}{dt} = L^{-1}(v_q - Ri_q - n_p L\omega i_d - n_p k_t \omega),$$

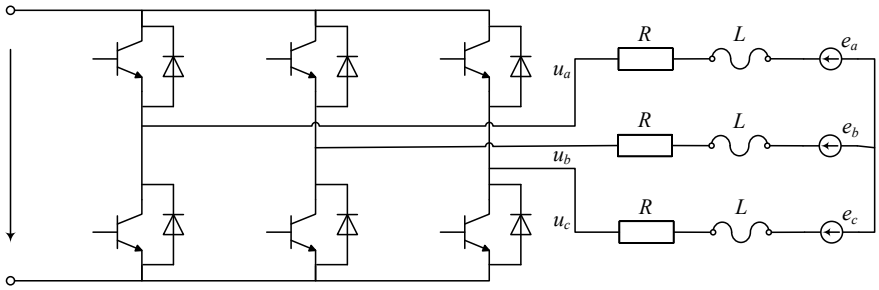

Fig. 1 Illustration of three-phase brushless motor with drive circuit

$$\frac{di_d}{dt} = L^{-1}(-Ri_d + n_p L_q \omega i_q + v_d),$$
$$\frac{d\omega}{dt} = J^{-1}(n_p k_t i_q - b\omega + T_{L0} + T_L \cos \Omega t) \tag{2}$$

where i_q and i_d are the quadrature-axis and direct-axis current; v_q and v_d are the quadrature-axis and direct-axis voltage; L is the fictitious inductance; R is winding resistance; n is number of pole pairs; ω is the rotor speed; J is the inertia of rotor; b is the viscous damping coefficient; T_L is the torque due to external load; T_L and Ω are the magnitude and frequency of the torque fluctuation due to the external load; $k_t = \sqrt{\frac{3}{2}} k_e$ and k_e is the permanent-magnet flux constant.

One define the state variables for such a motor as

$$\mathbf{x} \triangleq (x, y, z) \equiv (i_q, i_d, \omega) \tag{3}$$

For a period-1 motion of such a brushless motor system, it can be discretized into multiple mappings with constant time step. For a certain map P_k ($k = 0, 1, 2, \ldots$), it maps from one state $(x_{k-1}, y_{k-1}, z_{k-1})$ at $t = t_{k-1}$ to another (x_k, y_k, z_k) at $t = t_k$ with a mapping criteria based on the midpoint algorithm given as follows.

$$P_k : (x_{k-1}, y_{k-1}, z_{k-1}) \to (x_k, y_k, z_k) \Rightarrow (x_k, y_k, z_k) = P_k(x_{k-1}, y_{k-1}, z_{k-1}). \tag{4}$$

$$\begin{aligned} x_k &= x_{k-1} + hL^{-1}\big[v_q - R(x_{k-1} + x_k)/2 - n_p L(y_{k-1} + y_k) \\ &\quad (z_{k-1} + z_k)/4 - n_p k_t (z_{k-1} + z_k)/2\big], \\ y_k &= y_{k-1} + hL^{-1}\big[-R(y_{k-1} + y_k)/2 \\ &\quad + n_p L_q (x_{k-1} + x_k)(z_{k-1} + z_k)/4 + v_d\big], \\ z_k &= z_{k-1} + hJ^{-1}\big[n_p k_t (x_{k-1} + x_k)/2 - b(z_{k-1} + z_k)/2 \\ &\quad + T_{L0} + T_L \cos \Omega(t + dt/2)]. \end{aligned} \tag{5}$$

where $h = t_k - t_{k-1}$.

Then the mapping structure for such a period-m motion which is divided into mN partitions becomes

$$P = P_{mN} \circ P_{mN-1} \circ \cdots \circ P_2 \circ P_1 : (x_0, y_0, z_0) \to (x_{mN}, y_{mN}, z_{mN}). \tag{6}$$

Due to periodicity, the initial position for the first map and the final position of the final map should be overlapped, and the time span equals the time period of the external torque.

$$x_0 = x_N,\ y_0 = y_N \text{ and } t_N = t_0 + \frac{2\pi m}{\Omega} \tag{7}$$

For a period-m motion with mN maps, it has $3mN$ equations and the state variables for those nodes are unknown, the number of which is $3mN + 3$. But with the constraint given in Eq. (7), three more equations are added such that the node points for such a period-1 motion can be solved analytically through Newton-Raphson method.

To determine the stability of a period-1 motion, the small neighborhood of the node point $\mathbf{x}_k^*$ can be written as $\mathbf{x}_k = \mathbf{x}_k^* + \Delta\mathbf{x}_k$, $(k = 0, 1, 2, \cdots, N)$. Then linearize Eq. (6) at the equilibrium and the first order of the Taylor's expansion is kept, it gives

$$\Delta\mathbf{x}_N = DP\Delta\mathbf{x}_0 = \underbrace{DP_{mN} \cdot DP_{mN-1} \cdot \ldots \cdot DP_2 \cdot DP_1}_{mN-\text{multiplication}} \Delta\mathbf{x}_0 \tag{8}$$

where

$$DP_k = \left[\frac{\partial \mathbf{x}_k}{\partial \mathbf{x}_{k-1}}\right]_{(\mathbf{x}_k^*, \mathbf{x}_{k-1}^*)},\ \text{for } k = 1, 2, \cdots, N \tag{9}$$

Solve the Jacobian matrix **DP**, and it gives three eigenvalues such as λ_i $(i = 1, 2, 3)$. According to theory of the continuous system, the periodic motion is stable only if all of magnitudes of the eigenvalues are less than 1, e.g. $|\lambda_i| < 1$ ($i = 1$ and 2 and 3). Otherwise, the motion is unstable. At the boundary between the stable and unstable motions, it is the bifurcation point, of which the magnitude of one of the eigenvalues is 1:

I. If one of the eigenvalues is 1, the saddle-node bifurcation of period-1 motion occurs;
II. If one of the eigenvalues is -1, the period-doubling bifurcation of period-1 motion occurs;
III. If a pair of eigenvalues are complex with magnitude equating to 1, the Neimark bifurcation of period-1 motion occurs.

For a given resolution mN, a period-m motion can be divided into mN segments with constant time interval of mT/N where T is one period of excitation ($T = 2\pi/\omega$). Then a set of node points of periodic motions with $(mN + 1)$ points per one period of excitation can be expressed as. Furthermore, the set of node points of period-m motion with $(mN + 1)$ node points for one period can be expressed as

$$\Xi = \{(x_k, y_k, z_k) | t_k = t_0 + \frac{2k\pi}{N\Omega}; t_0 = 0; k = 0, 1, 2, \ldots, mN\} \tag{10}$$

Instead of presenting all node points of periodic motions, the node points per each period of excitation frequency are collected in the Poincaré mapping section for period-1 motions. Such Poincaré mapping is defined as

$$\Xi_{PM} = \{ (x_k, y_k, z_k) | \bmod (k, N) = 0, \tau_k = \tau_0 + \frac{kT}{N}; \\ \tau_0 = 0; k = 0, 1, 2, \ldots, mN\} \tag{11}$$

By analyzing the aforementioned set Ξ via Discrete Fourier Transform, the analytic solution for such a period-m motion can be recovered as

$$\mathbf{x}(t) \approx \mathbf{a}_0^{(m)} + \sum_{j=1}^{mN/2} \mathbf{b}_{j/m} \cos(\tfrac{j}{m}\Omega t) + \mathbf{c}_{j/m} \sin(\tfrac{j}{m}\Omega t) \tag{12}$$

and

$$\mathbf{a}_0^{(m)} = \frac{1}{mN} \sum_{k=0}^{mN-1} \mathbf{x}_k, \\ \mathbf{b}_{j/m} = \frac{2}{mN} \sum_{k=0}^{mN-1} \mathbf{x}_k \cos(\tfrac{j}{m}\Omega t_k), \\ \mathbf{c}_{j/m} = \frac{2}{mN} \sum_{k=0}^{mN-1} \mathbf{x}_k \sin(\tfrac{j}{m}\Omega t_k), \\ t_k = \frac{2k\pi}{\Omega mN}, \tag{13}$$

where $\mathbf{a}_0^{(m)} = (a_{01}^{(m)}, a_{02}^{(m)}, a_{03}^{(m)})$, $\mathbf{b}_{j/m} = (b_{j/m(1)}, b_{j/m(2)}, b_{j/m(3)})$ and $\mathbf{c}_{j/m} = (c_{j/m(1)}, c_{j/m(2)}, c_{j/m(3)})$.

The highest order of the harmonic depends on the number of the partition which the motion is divided into. The amplitude and phase for each order of harmonic for the period-1 motion are expressed by

$$\mathbf{A}_{k/m} = \sqrt{\mathbf{b}_{k/m}^2 + \mathbf{c}_{k/m}^2}, \ \varphi_{k/m} = \arctan \frac{c_{k/m}}{b_{k/m}} \tag{14}$$

3 Analytical Bifurcation

For an eight-pole brushless motor, the system parameters are given as

$$R = 0.9, n_p = 4, L = 0.01425, k_t = 0.031, \xi = 0.0162, J = 0.000047 \tag{15}$$

For the loading condition, it is assumed as $T_{L0} = 0$, $T_L = 0.2$ and $\Omega = 10$. The quadrature-axis voltage v_q is set to be zero and direct-axis voltage v_d is varied from -9.0 V to -6.0 V. The analytical bifurcation diagram of node point sets of period-1 motion, which is expressed as in Eq. (10), for such a brushless motor is illustrated in Fig. 2. The solid curve is stable motion and the dashed curved is unstable motion. For the upper branch of the stable period-1 solution, the periodic nodes of the states for such a brushless motor system (such as quadratic-axis current, direct-axis current, and rotation speed) are almost invariant when the direct-axis voltage increases. The period-doubling bifurcation ("PD") of the period-1 motion occurs at $v_d = -7.769$ V, and the saddle-node bifurcation ("SN") of the period-1 motion is at $v_d = -7.752$ V.

Since the rotor speed is the mechanical state, by which the vibration of such a brushless motor can be affected it can reflect the vibration characteristics of such a brushless motor, the harmonic amplitudes of rotor speed for such a motor when the direct-axis varies in the range of $v_d \in [-9, -6]$ are presented In Fig. 3. The constant terms a_{03} gives the average value of the rotor speed versus direct-axis voltage, which is shown in Fig. 3a. For constant term a_{03} which is nonzero, the periodic motion is asymmetric to the rotor speed. Otherwise, the periodic motion is symmetric to the rotor speed. In Figs. 3b–d, the first three orders of the harmonic amplitudes are illustrated. For the analytical solution of the periodic motion which is symmetric to the rotor speed, the even orders of the harmonic amplitude for $A_{k(3)}$ ($k = 2, 4, 6, \ldots$) are all zero. It can be seen that the third order of the harmonics for the period-1 motions still has a quantity level of 10^1, which indicates that higher orders of harmonic are required. The harmonic amplitude of $A_{2(3)}$ goes to zero at $v_d = -7.557$ V which is the unstable saddle-node bifurcation, and the unstable periodic solution has jump phenomenon when the direct-axis voltage continues to increases. In Figs. 3e, f, the harmonic amplitudes of $A_{59(3)}$ and $A_{60(3)}$ are shown, respectively. The quantity level of harmonic amplitude for stable period-1 motion which is asymmetric to rotor speed has dropped to 10^{-4} when the order increases to 60, and the quantity level of harmonic amplitude for stable period-1 motion which is symmetric to rotor speed has dropped to 10^{-2} when the order increases to 59.

For period-2 motion, it only exists in a very narrow range. The periodic nodes for period-2 motion in the range of $v_d = [-7.764, -7.745]$ are shown in Fig. 4. The period-doubling bifurcation occurs at $v_d = -7.752408$ V and -7.754412 V. In Fig. 5a, for the constant term a_{03} of stable period-2 motion, it increases and then decreases when the direct-axis voltage increases. But the average rotation speed only varies from 9.452250 to 10.632700 rad/s. For the period-2 motion, the subharmonic terms of $A_{k/2(3)}$ ($k = 1, 3, 5, \ldots$) is non-zero, as shown in Fig. 5b–g. For $k = 6$, the harmonic amplitude still has a quantity level of 10^1. For $k = 94$ and 95 which is shown in Fig. 5h, i, the quantity level decreases to 10^{-2}, and it becomes 10^{-3} when $k = 96$ as is given in Fig. 5j.

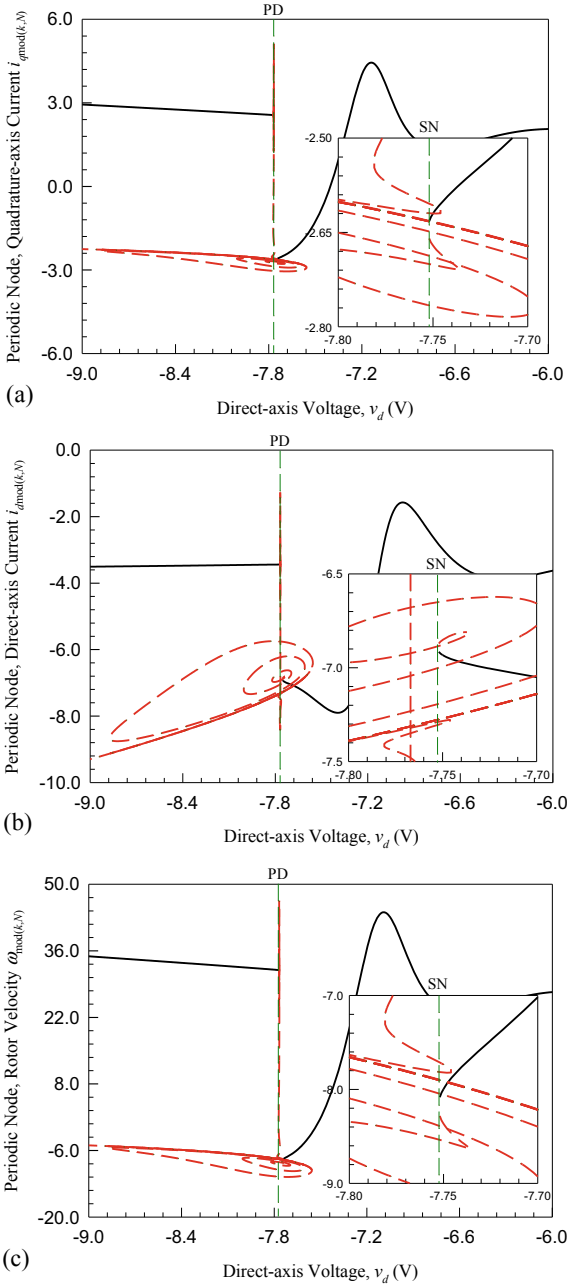

Fig. 2 Analytical bifurcation of periodic nodes of period-1 motion for brushless motor ($R = 0.9$, $n_p = 4$, $L = 0.01425$, $k_t = 0.031$, $\xi = 0.0162$, $J = 0.000047$) with working condition $T_{L0} = 0$, $T_L = 0.2$, $\Omega = 10$ and $v_q = 0$: **a** quadrature-axis current, **b** direct-axis current and **c** rotor velocity

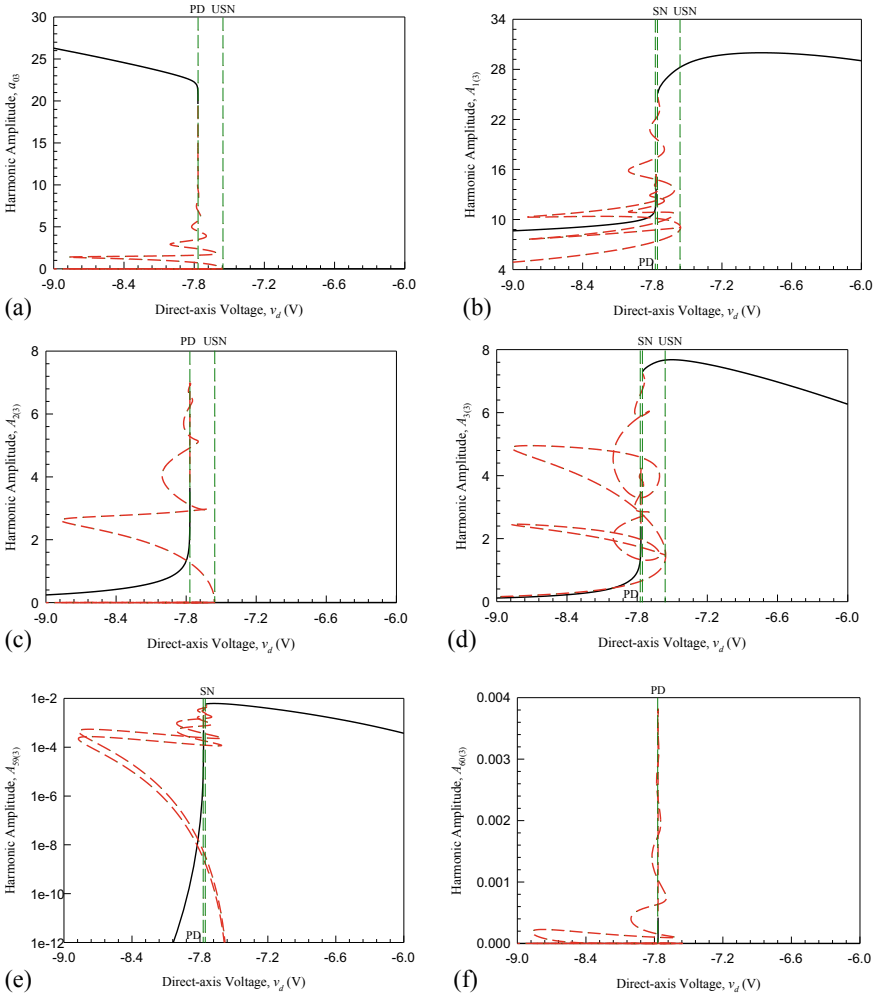

Fig. 3 Harmonic amplitude of rotor speed for brushless motor ($R = 0.9$, $n_p = 4$, $L = 0.01425$, $k_t = 0.031$, $\xi = 0.0162$, $J = 0.000047$) with working condition $T_{L0} = 0$, $T_L = 0.2$, $\Omega = 10$ and $v_q = 0$: **a** constant term, **b–d** first three orders of harmonics, **e** harmonic amplitude of $A_{59(3)}$ and **f** harmonic amplitude of $A_{60(3)}$

4 Periodic Motions

In this section, periodic motions in the brushless motor with loading fluctuation will be discussed. The initial conditions are calculated by the analytical solution which is obtained through implicit discrete map method at the phase $t = 0$ which is given by the green solid circle ("I.C."). The solid curve is the numerical prediction, and the red fork symbols are the analytical solution.

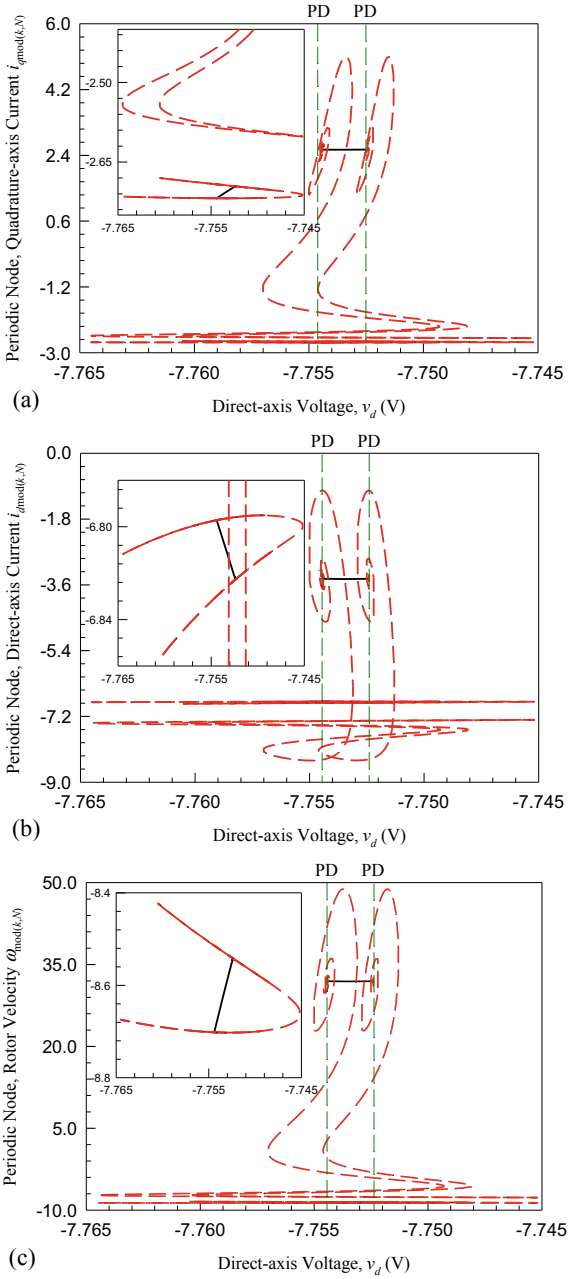

Fig. 4 Analytical bifurcation of periodic nodes of period-2 motion for brushless motor ($R = 0.9$, $n_p = 4$, $L = 0.01425$, $k_t = 0.031$, $\xi = 0.0162$, $J = 0.000047$) with working condition $T_{L0} = 0$, $T_L = 0.2$, $\Omega = 10$ and $v_q = 0$: **a** quadrature-axis current, **b** direct-axis current and **c** rotor velocity

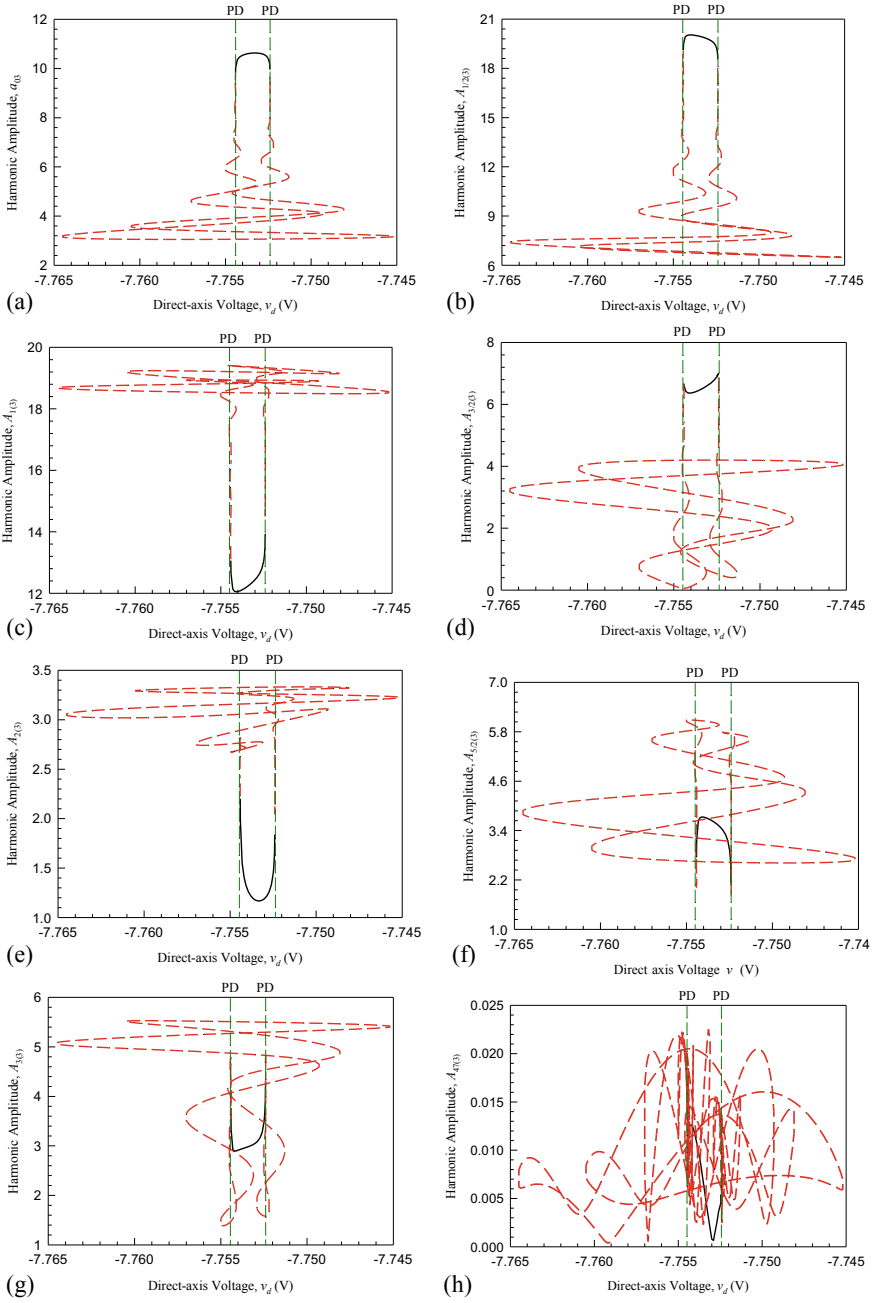

Fig. 5 Harmonic amplitude of rotor speed of period-2 motions for brushless motor ($R = 0.9$, $n_p = 4$, $L = 0.01425$, $k_t = 0.031$, $\xi = 0.0162$, $J = 0.000047$) with working condition $T_{L0} = 0$, $T_L = 0.2$, $\Omega = 10$ and $v_q = 0$: **a** constant term, harmonic amplitudes of **b** $A_{1/2(3)}$, **c** $A_{1(3)}$, **d** $A_{3/2(3)}$, **e** $A_{2(3)}$, **f** $A_{5/2(3)}$, **g** $A_{3(3)}$, **h** $A_{47(3)}$, **i** $A_{95/2(3)}$, **j** $A_{48(3)}$

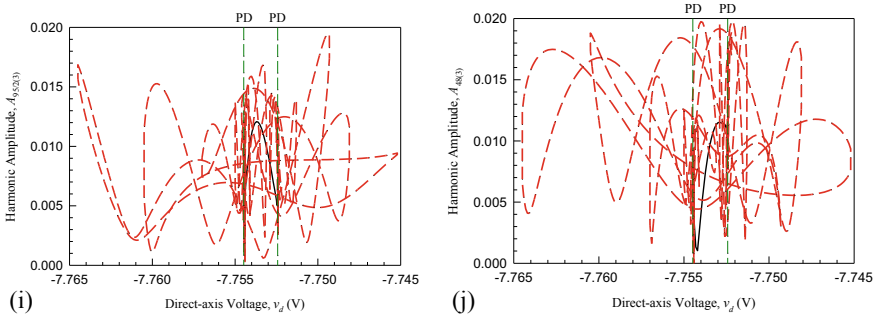

Fig. 5 (continued)

A stable period-1 motion at $v_d = -7.73$ V is presented in Fig. 6a–c, and the initial conditions are $(i_{q0}, i_{d0}, \omega_0) \approx (-2.558350, -6.994479, -7.567532)$. It can be found that the numerical simulation correlates with the analytical solution very well. In Fig. 6b, the rotor speed versus time is illustrated and one period is labeled. For the harmonic amplitudes of the rotor speed, which are presented in Fig. 6c, the constant term is zero and the first harmonic is 25.9979 rad/s. The amplitudes of even orders ($A_{k(3)}$ for $k = 2, 4, 6, \ldots$) for such a stable period-1 motion are all zero, and the amplitudes of the order orders drop asymptotically with the increase of the order. The harmonic amplitude stay above 1 for $k < 21$, and the quantity level drops to 10^{-2} until $k = 39$. The quantity level goes to 10-4 when k increases to 73. With the same system parameters, there is another unstable motion coexisted which is presented in Figs. 6d–f. The initial conditions for such a unstable period-1 motion are given as $(i_{q0}, i_{d0}, \omega_0) \approx (-2.779143, -6.624351, -9.195011)$, for which the initial current for quadratic-axis and direct-axis is very close to those for the aforementioned stable period-1 motion. As shown in Fig. 6e, the numerical prediction stay on the unstable period-1 orbit for the first half cycle and then leaves due to the error accumulation of the numerical simulation and the strong attraction of the stable orbit. In order to illustrate all the coexisting periodic motions at $v_d = -7.73$, the analytical solutions of the stable and unstable motions are plotted in Fig. 7. The black solid curve is the stable period-1 motion, and there are other six unstable period-1 motions which are represented by the color dashed curves.

In Fig. 8, a stable and unstable period-2 motion at $v_d = -7.754$ V are demonstrated. As shown in Fig. 8c, f, the frequency spectrum for period-2 motions becomes more dense than that for period-1 motion since the subharmonics such as $A_{k/2(3)}$ ($k = 1, 3, 5, \ldots$) are introduced. There are one stable period-2 motion and eight unstable period-2 motions coexisting at $v_d = -7.754$ V which is plotted in Fig. 9. It can be found that the lower part of all the periodic motions is almost overlapped.

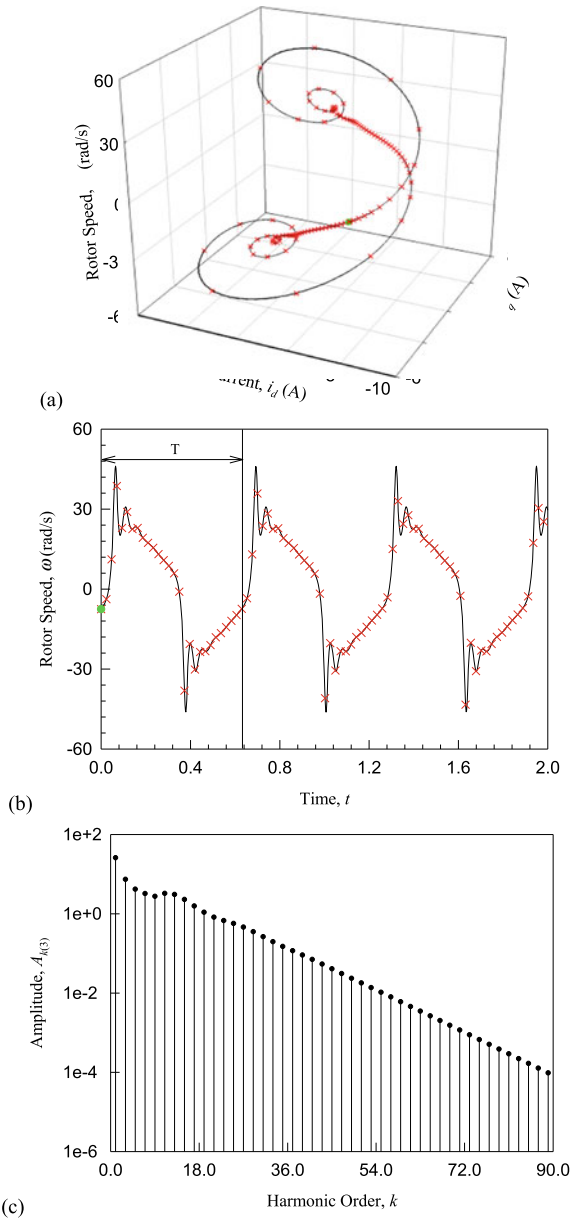

Fig. 6 Period-1 motion for $v_d = -7.73$: stable motion **a** 3-D trajectory **b** time history of rotation speed ω, **c** harmonic amplitude of $A_{k(3)}$ (initial conditions: $(i_{q0}, i_{d0}, \omega_0) \approx (-2.558350, -6.994479, -7.567532)$; unstable motion **d** 3-D trajectory **e** time history of rotation speed ω, **c** harmonic amplitude of $A_{k(3)}$ (initial conditions: $(i_{q0}, i_{d0}, \omega_0) \approx (-2.779143, -6.624351, -9.195011)$, $(R = 0.9,\ n_p = 4,\ L = 0.01425,\ k_t = 0.031,\ \xi = 0.0162,\ J = 0.000047)$

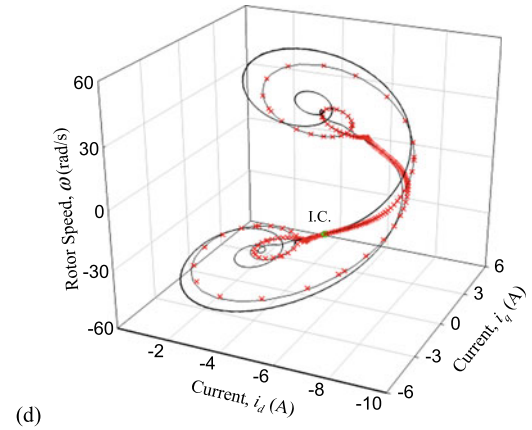

(d)

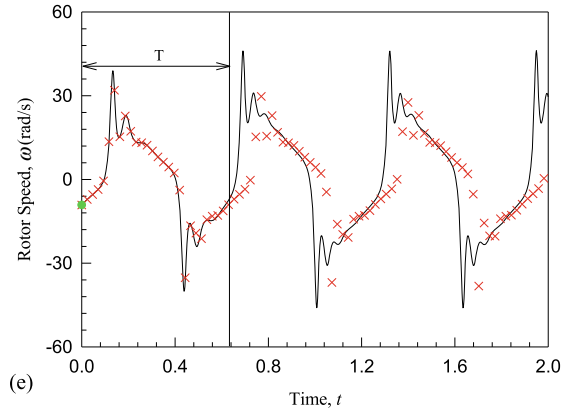

(e)

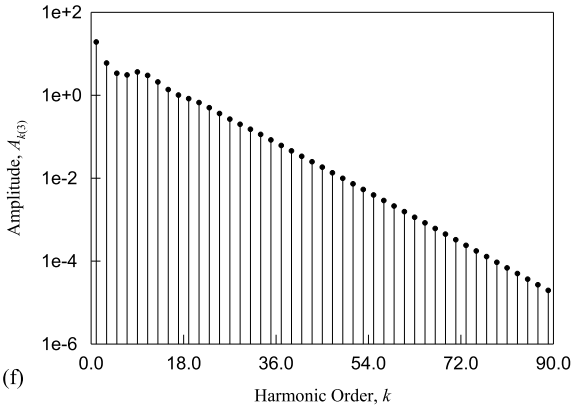

(f)

Fig. 6 (continued)

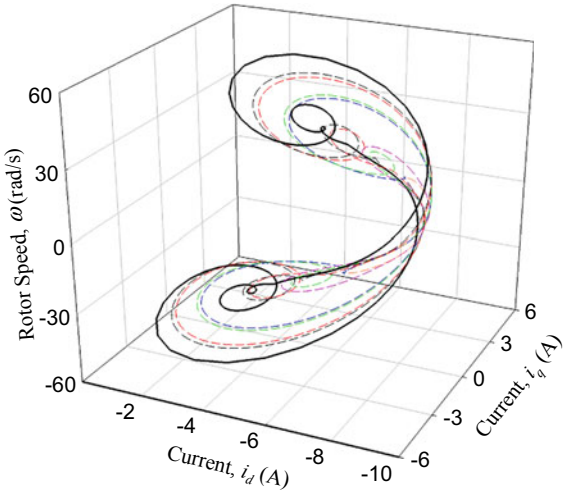

Fig. 7 Coexisting analytical orbits for period-1 motions for $v_d = -7.73$ ($R = 0.9,\ n_p = 4,\ L = 0.01425,\ k_t = 0.031,\ \xi = 0.0162,\ J = 0.000047$)

5 Conclusions

In this chapter, the discrete implicit maps method is adopted to investigate the nonlinear dynamic behavior of a brushless motor. A periodic torque is introduced to model the loading fluctuation. Period-*m* motion is discretized and mappings are described using a set of algebraic equations. Through Newton-Raphson method, the node points of mappings of period-1 motion for such a brushless motor can be easily solved and the eigenvalue analysis has been carried out through the reduced system. By selecting specific parameters, analytic bifurcation for Poincaré section and solution of period-1 motion varying direct-axis voltage have been presented. A strong nonlinear characteristic for such a brushless motor with periodically excited loading can be observed, and higher orders of harmonics should be kept in the solution which may be difficult to solve for traditional analytical method of solving nonlinear problems such as harmonic balance method. With such a technique, many coexisting unstable periodic motions can be obtained, and with proper control such unstable periodic motions can be altered to be stable if the motions are desired for operation.

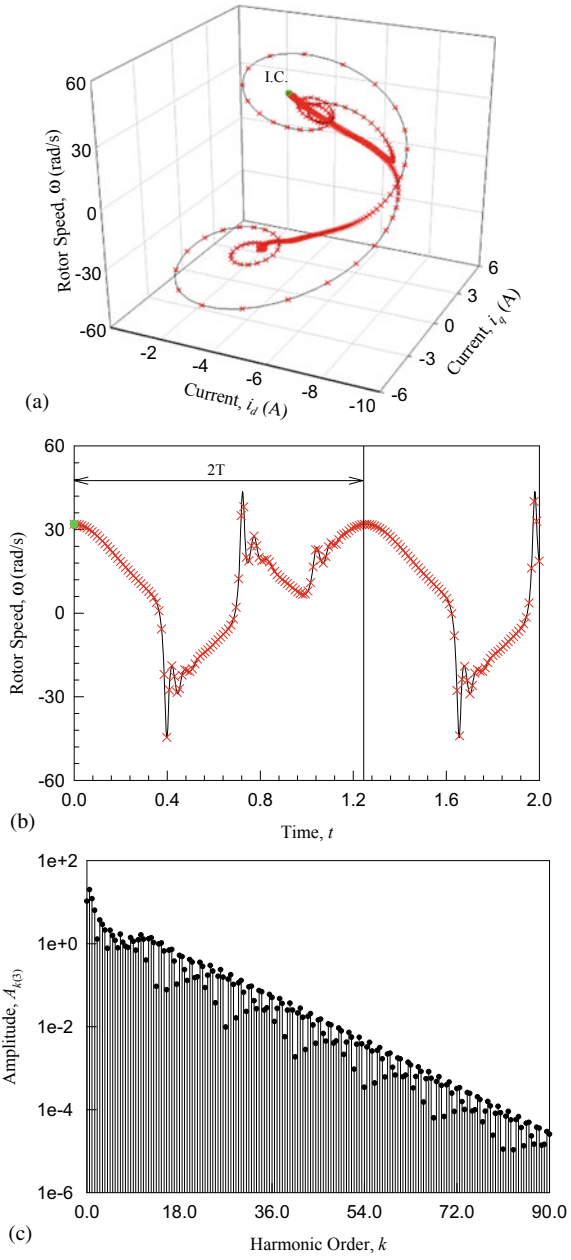

Fig. 8 Period-2 motion for $v_d = -7.754$: stable motion **a** 3-D trajectory **b** time history of rotation speed ω, **c** harmonic amplitude of $A_{k(3)}$ (initial conditions: $(i_{q0}, i_{d0}, \omega_0) \approx$ (2.557057, -3.437199, 31.922249); unstable motion **d** 3-D trajectory **e** time history of rotation speed ω, **c** harmonic amplitude of $A_{k(3)}$ (initial conditions: $(i_{q0}, i_{d0}, \omega_0) \approx (-.582655, -8.315973, 5.041553), R = 0.9,\ n_p = 4,\ L = 0.01425,\ k_t = 0.031,\ \xi = 0.0162,\ J = 0.000047$)

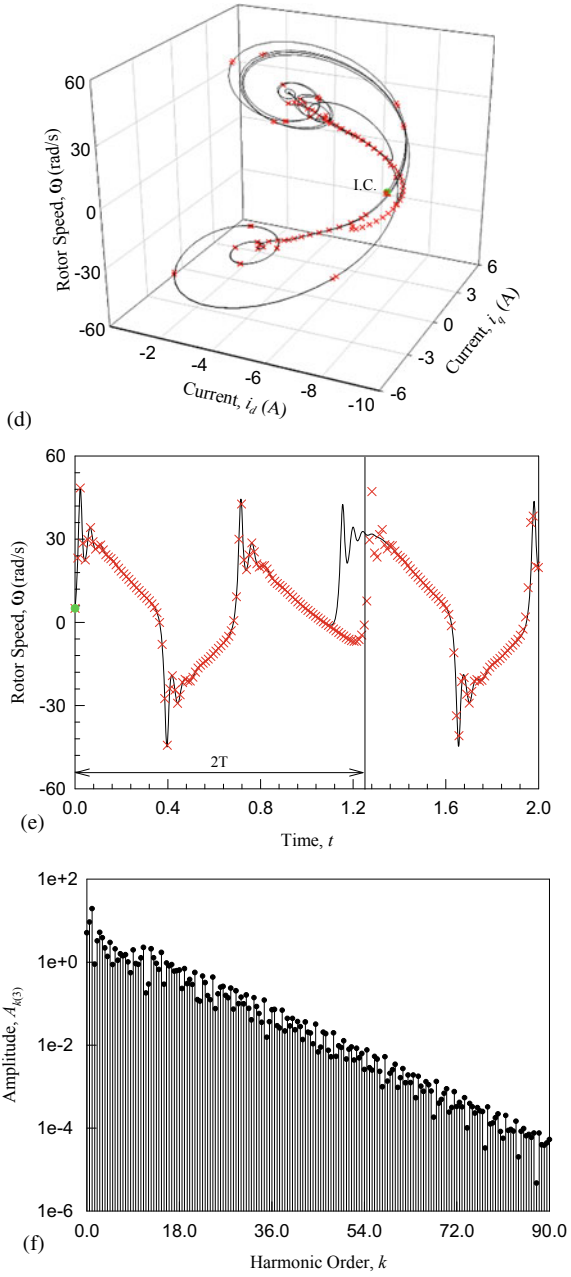

Fig. 8 (continued)

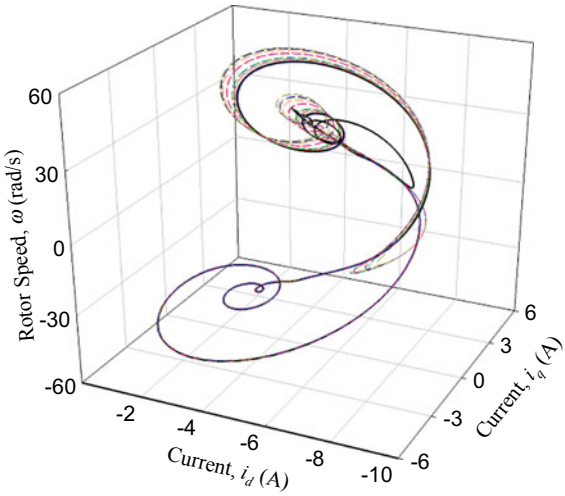

Fig. 9 Coexisting analytical orbits for period-1 motions for $v_d = -7.754$ ($R = 0.9,\ n_p = 4, L = 0.01425,\ k_t = 0.031,\ \xi = 0.0162,\ J = 0.000047$)

References

1. Hemati N (1992) The global and local dynamics of direct-drive brushless dc motors. In: the 1992 IEEE International conference on robotics and automation. Nice, France, May 12–14
2. Hemati N (1993) Dynamic analysis of brushless motors based on compact representations of equations of motion. In: the 1993 IEEE industry applications conference 28th IAS annual meeting. Toronto, Canada, October 2–8
3. Kang SJ, Sul SK (1995) Direct torque control of brushless dc motor with nonideal trapezoidal back EMF. IEEE Trans Power Electron 10(6):796–802
4. Rubaai A, Kotaru R, Kankam MD (2000) A continually online-trained neural network controller for brushless dc motor drives. IEEE Trans Ind Appl 36(2):475–483
5. Ge ZM, Chang CM (2004) Chaos synchronization and parameters identification of single time scale brushless dc motors. Chaos Solitons Fractals 20(4):883–903
6. Lee BK, Ehsani M (2003) Advanced simulation model for brushless dc motor drives. Electr Power Compon Syst 31(9):841–868
7. Jabbar MA, Phyu HN, Liu ZJ, Bi C (2004) Modeling and numerical simulation of a brushless permanent-magnet dc motor in dynamic conditions by time-stepping technique. IEEE Trans Ind Appl 40(3):763–770
8. Luo Shaohua, Wang Jiaxu, Songli Wu (2014) Chaos RBF dynamics surface control of brushless dc motor with time delay based on tangent barrier Lyapunov function. Nonlinear Dyn 78(2):1193–1204
9. Zhang F, Lin D, Xiao M, Li H (2014) Dynamical behaviors of the chaotic brushless dc motors model. Complexity 21(4):79–85
10. Luo S, Wu S, Gao R (2015) Chaos control of the brushless direct current motor using adaptive dynamic surface control based on neural with the minimum weights. Chaos 25(7) 073102:8
11. Jagiela M, Gwozdz J (2015) Steady-state time-periodic finite element analysis of a brushless dc motor drive considering motion. Arch of Electr Eng 64(3):471–486
12. Cho S, Hwang J, Kim CW (2018) A study on vibration characteristics of brushless dc motor by electromagnetic-structural coupled analysis using entire finite element model. IEEE Trans Energy Convers. https://doi.org/10.1109/TEC.2018.2833493

13. Hayashi G (1964) Nonlinear oscillations in physical systems. McGraw-Hill Book Company
14. Nayfeh AH, Singh V (1978) Perturbation methods. IEEE Trans Syst Man Cybern 8(4):417–418
15. Luo ACJ, Huang JZ (2013) Analytical solutions for asymmetric periodic motion to chaos in a hardening Duffing oscillator. Nonlinear Dyn 72(1–2):417–438
16. Huang JZ, Luo ACJ (2015) Periodic motions and bifurcation trees in a buckled, nonlinear Jeffcott rotor system. Int J Bifurc Chaos 25(1):1550002
17. Luo ACJ (2015) Periodic flows in nonlinear dynamical systems based on discrete implicit maps. Int J Bifurc Chao 25, 1550044: 62
18. Wang D, Huang JZ (2016) Periodic motions and chaos for a damped mobile piston system in a high pressure gas cylinder with P control. Chaos Solitons Fractals 95:168–178
19. Luo ACJ, Xing SY (2016) Multiple bifurcation tress of period-1 motions to chaos in a periodically forced, time-delayed, hardening Duffing oscillator. Chaos Solitons Fractals 89:405–434
20. Guo Y, Luo ACJ (2017) Period-1 motions to chaos in a parametrically excited pendulum. In: ASME 2017 International mechanical engineering congress and exposition. Tampa, USA, November 3–9